Eur. J. Biochem. 218, 853–860 (1993)

^{1}H-NMR studies and secondary structure of the RGD-containing snake toxin, albolabrin

Mahesh JASEJA[1], K. John SMITH[1], Xinjie LU[2], Janice A. WILLIAMS[3], Hylary TRAYER[1], Ian P. TRAYER[1] and Eva I. HYDE[1]

[1] School of Biochemistry, University of Birmingham, England
[2] Thrombosis Research Institute, Emmanuel Kaye Building, London, England
[3] Department Applied Pharmacology, National Heart and Lung Institute, London, England

(Received August 2/September 30, 1993) – EJB 93 1169/2

Albolabrin is a naturally occurring peptide from snake venom containing the sequence Arg-Gly-Asp (RGD). It inhibits platelet aggregation by blocking the binding of fibrinogen to the glycoprotein Gp IIb-IIIa, on the surface of activated platelets. Albolabrin consists of 73 residues with six intramolecular disulphide bonds. The ^{1}H-NMR spectrum of albolabrin has been assigned using homonuclear two-dimensional techniques and its secondary structure determined. Like kistrin and echistatin, two related peptides from snake venom, albolabrin appears to have little regular secondary structure in solution. Several bends and two short distorted β sheets are observed. The RGD sequence, important for binding to the receptor, lies in a mobile loop joining two strands of one of these β sheets. This loop undergoes a pH-dependent conformational change.

RGD-containing cysteine-rich peptides isolated from snake venoms recently have been shown to be potent inhibitors of the binding of fibrinogen to activated platelets and hence of platelet aggregation (Dennis et al., 1990; Gould et al., 1990). The Arg-Gly-Asp (RGD) sequence has been found to be the consensus sequence by which adhesive proteins such as fibrinogen, fibronectin, vitronectin and von Willebrand factor recognise the glycoprotein Gp IIb-IIIa complex, which is the major receptor for fibrinogen on activated platelets (Ruoslahti and Pierschbacher, 1987). Small synthetic peptides which contain the RGD sequence compete with fibrinogen in binding to Gp IIb-IIIa and so have been studied as potential antithrombotic agents (Plow et al., 1985, 1987; Gartner and Bennett, 1985; Samanen et al., 1991). The RGD sequence is also involved in the binding of adhesive proteins to other cell surface integrins, such as $\alpha_5\beta_1$ in fibroblasts and $\alpha_v\beta_1$ in endothelial cells. The strength of inhibition of platelet aggregation by the snake venom disintegrins is much higher than that of the small synthetic peptides, and they show greater selectivity for integrins. This may be due to the precise conformation of the RGD peptide, to the amino acids adjacent to the consensus sequence or to the tertiary structure of the disintegrin. In order to understand the specificity of various RGD-containing peptides, and the molecular mechanisms by which these ligands bind to the integrins, it is necessary first to examine their structures in solution.

A large number of disintegrins have now been sequenced (Huang et al., 1989; Gould et al., 1990; Williams et al., 1990b; Scarborough et al., 1993). They fall into three families: the long 83–84-residue peptides with 14 Cys residues, the medium 68–73-residue peptides with 12 Cys, and the short 48–49-residue aminoacid peptides with 8 Cys. The sequences of the peptides are highly similar and, within a family, the positions of the RGD sequence and of the Cys are conserved. The Cys are all disulphide-bonded and reduction results in decrease of biological activity (Huang et al., 1987; Gan et al., 1988; Williams, 1992). Despite this conservation, the disulphide-bonding pattern for kistrin and flavoridin appears to differ from that of albolabrin, although all are medium-length peptides (Calvete et al., 1991, 1992; Adler et al., 1993; Klaus et al., 1993) and that of echistatin, a short peptide, differs again (Cooke et al., 1992; Calvete et al., 1992). This surprising difference has made the identity of the disulphide bridges within the disintegrins controversial. The structures of three disintegrins, kistrin, echistatin, and flavoridin, have been determined by NMR spectroscopy (Adler et al., 1991; Adler and Wagner, 1992; Cooke et al., 1991, 1992; Chen et al., 1991; Dalvit et al., 1991; Saudek et al., 1991a, b; Senn and Klaus, 1993). In this paper we present the assignments of the ^{1}H-NMR spectrum and the secondary structure of albolabrin.

MATERIALS AND METHODS

Peptide isolation

Albolabrin was isolated from the venom of the viper *Trimerusurus albolabris*, purchased from Latoxan (France). It was purified by reverse-phase high-pressure liquid chromatography using a modification of the method of Williams et al. (1990b). 100 mg of whole lyophilised venom protein was dissolved in 0.5 ml 0.1% trifluoroacetic acid, left for 10 min on ice, and microfuged for 2 min to remove any insoluble material. The supernatant was adsorbed onto a preparative, 22×250 mm, wide-pore 10-μm C_{18} silica reverse-phase col-

Correspondence to E. I. Hyde, School of Biochemistry, University of Birmingham, Edgbaston, Birmingham, England B15 2TT

Abbreviations. DQF-COSY, double-quantum-filtered correlation spectroscopy; MLEV 17, isotropic mixing sequence based on a sequence described by M. Levitt; NOESY, nuclear Overhauser enhancement spectroscopy; TOCSY, total correlation spectroscopy; TPPI, time-proportional phase incrementation.

umn (Vydac 218TP) and eluted with a gradient of 0.1% trifluoroacetic acid containing 0–16% acetonitrile (1.6% min^{-1}) followed by 16–35% acetonitrile (0.45% min^{-1}). The fractions were freeze-dried, dissolved in H_2O and assayed for the inhibition of ADP-induced platelet aggregation. Active fractions were pooled, trifluoroacetic acid was added to 0.1%, and the pool was repurified on an analytical, 4×250 mm, 5 μm C_2/C_{18} column (Pharmacia) with a similar gradient. If necessary, further analytical columns were run under similar conditions. Albolabrin eluted at 28% acetonitrile with an overall yield of 0.3–0.4%. Purified albolabrin was characterised by its IC_{50} in the platelet aggregation assay. Platelet-rich plasma was prepared and platelet aggregation assays performed as described by Williams et al. (1990a, b).

Sedimentation equilibrium

These studies were performed with a model E analytical ultracentrifuge (Beckmann Instruments Co.) equipped with Rayleigh interference optics. All experiments were performed using an An-D rotor and a 12-mm double-sector capillary synthetic-boundary cell fitted with sapphire windows. The long-column meniscus-depletion equilibrium method was used as described by Chervenka (1970). Equilibrium was established by ascertaining that no further fringe displacement occurred with time. The Rayleigh patterns were photographed on Kodak type II-G spectroscopic plates. The fringe displacement (f) as a function of radial distance (r) was measured with a Nikon two-dimensional microcomparator. All fringe displacements greater than 100 μm were included in the least-squares analysis. The mass-average molecular mass (M_m) for the whole solution was then calculated from the equation:

$$M_m = 2\times10^{-3}[RT/\omega^2(1-v\rho)] \cdot d\ln f/r^2$$

where R is the gas constant (in $J \cdot K^{-1} \cdot mol^{-1}$), ω is the angular velocity (rad $\cdot s^{-1}$), v is the partial specific volume of the protein, ρ is the density of the solvent, f is the fringe displacement and r is the distance from the centre of rotation (in m).

The concentration of albolabrin in the solution, was determined from the total fringe shift across the boundary (Babul and Stellwagen, 1969). A solution of albolabrin at 3 mg $\cdot$ ml^{-1} in water at pH 5, 298 K, was used for these measurements. The density of water was assumed to be 1.0 g $\cdot$ ml^{-1} and a v of 0.7 g^{-1} $\cdot$ ml was calculated from the amino acid composition (Cohn and Edsall, 1943). Initially a speed of 52600 rpm was used and equilibrium was attained in 6–8 h. The speed was subsequently increased to 55993 rpm and photographs taken after a further 14 h centrifugation.

NMR samples

Samples for NMR were prepared by dissolving lyophilised albolabrin in 100% D_2O or in 90% H_2O/10% D_2O to a concentration of under 2 mM. NMR experiments were carried out at several pH values between 4.5–7.0 and temperatures between 295–310 K. Above 310 K many of the amide proton resonances disappeared, whereas below 295 K spectral overlap and broadening of the resonances made their assignment difficult. The pH values were adjusted using small volumes of acid or base.

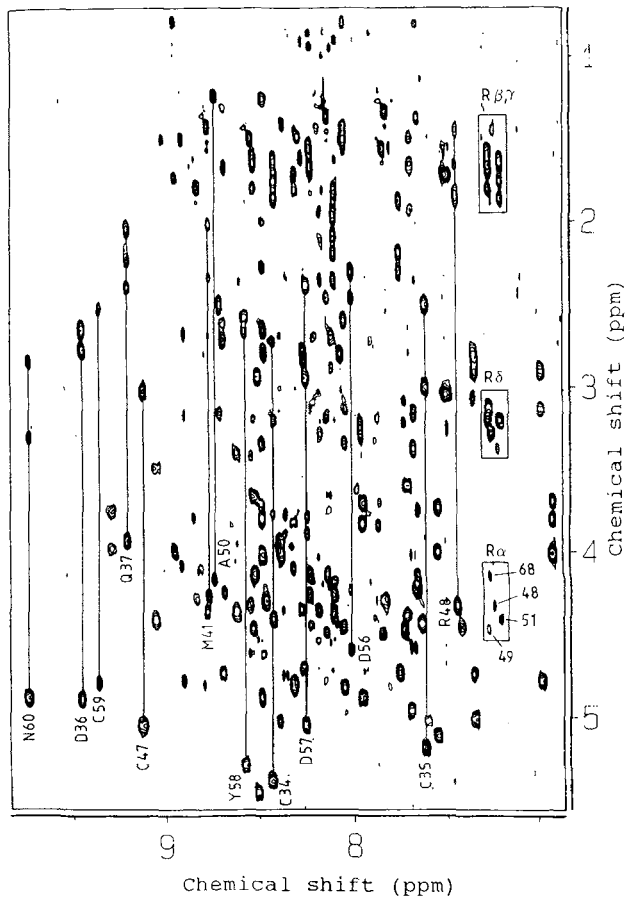

Fig. 1. NH-aliphatic region of the TOCSY spectrum of albolabrin dissolved in 90% H_2O/10% D_2O, pH 4.5, 310 K. The spin-lock mixing time was 65 ms. Selected connectivities from amide protons to side-chain protons are indicated by straight lines. The connectivities from the arginine NεH to the side chains are boxed.

NMR spectra were recorded on a Bruker AMX-500 spectrometer. All spectra were recorded with presaturation of the solvent resonance for 1.5 s. Two-dimensional double-quantum-filtered correlation spectroscopy (DQF-COSY; Piatini et al., 1982; Shaka and Freeman, 1983; Rance et al., 1983), nuclear Overhauser spectroscopy (NOESY; Jeener et al., 1979; Kumar et al., 1980) and total correlation spectroscopy (TOCSY; Braunschweiler and Ernst, 1983) experiments were performed in phase-sensitive mode, using the time-proportional phase incrementation (TPPI) method for quadrature detection in f_1 (Marion and Wuthrich, 1983). The mixing times in the NOESY and the TOCSY experiments ranged over 100–200 ms and 40–60 ms. The spin-lock period in the TOCSY was achieved using the MLEV-17 pulse sequence (Bax and Davis, 1985) with a spin-lock field of 8 kHz. Typically, 2 K complex data points were acquired for each of 400–500 increments over a spectral width of 5500 Hz. The data were zero-filled in the f_1 dimension to 1 K points and in the f_2 dimension to 2 K points prior to Fourier transformation. Spectra were processed on a Bruker X-32 computer using UXNMR software with shifted-sine-bell window functions and baseline correction in both dimensions. The $^3J_{HNH\alpha}$ coupling constants were estimated from the separation of cross-peak components in a DFQ-COSY spectrum with a digital resolution of 0.63 Hz/point. All the chemical shifts were referenced to the methyl resonance of

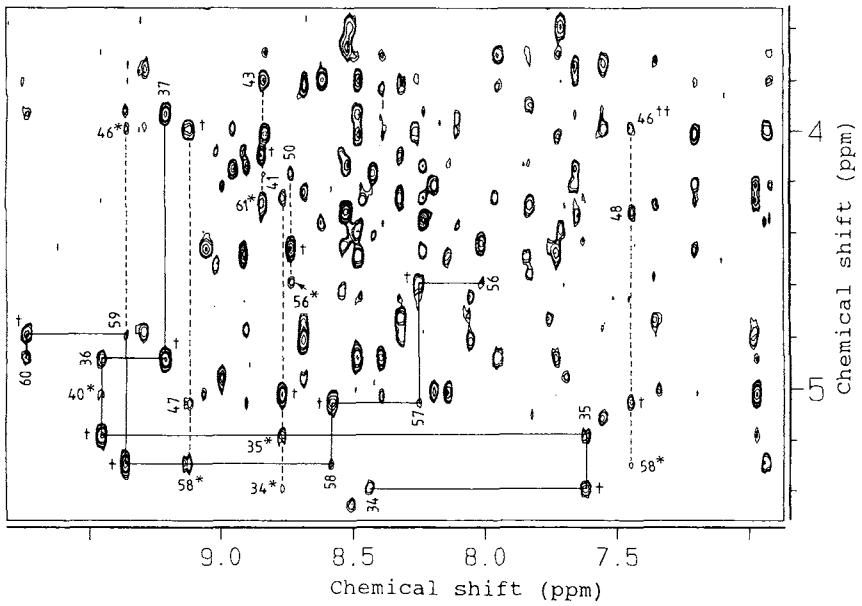

Fig. 2. NH/CαH 'fingerprint' region of the NOESY spectrum of albolabrin dissolved in 90% H_2O/10% D_2O, pH 4.5, 310 K. The mixing time was 150 ms. The sequential connectivities between residues C34–Q37 and D56–N60, including the unique Tyr at 58, are shown in solid lines. These residues form strands of β sheet. Intraresidual NOEs are indicated by numbers while sequential NOEs are indicated by a cross (†). All long-range NH-CαH connectivities across the strands of these sheets are shown with dotted lines and labelled with an asterisk (*). The αN (i,i+2) NOE between Ile46 and Arg48 is shown with two crosses (††).

trimethylsilylpropionate at 0 ppm, added as an internal reference.

To determine which of the amide protons exchanged very slowly, 10 mM sodium phosphate buffer was added to the sample in H_2O and its pH was adjusted to 6.5. The sample was freeze-dried, redissolved in D_2O, and one-dimensional spectra were recorded after 5 min and after 30 min. To assign the amide resonances, two-dimensional TOCSY spectra were recorded over 3–4 h and overnight.

RESULTS AND DISCUSSION

Ultracentrifugation experiments

The first step in the study of the peptide was the determination of its molecular mass. Albolabrin has a large number of acidic residues with a calculated pI of 4.6 and migrates anomalously in SDS/PAGE. It was therefore important to determine whether it was monomeric or dimeric in solution. Equilibrium ultracentifugation was used to determine the molecular mass under NMR solution conditions. At 52600 rpm, a molecular mass of 8400 Da was determined while at 55993 rpm the molecular mass was calculated to be 8300 Da. The subunit mass calculated from the amino acid composition is 7648.3 Da. At neither speed was there any indication of dimerisation of the peptide; thus all the NOEs observed in the NMR studies are intramolecular.

Assignment of the NMR spectra

Assignment of the ^{1}H-NMR specrum was achieved using the conventional strategy of first identifying the individual amino acid spin systems using COSY and TOCSY, establishing connectivities between neighbouring residues by NOESY and matching these connecting segments to the known protein sequence (Wuthrich, 1986).

The spin systems of the individual amino acids were assigned by comparison of the TOCSY spectra with DFQ-COSY spectra in both H_2O and D_2O (Fig. 1). The spin systems of the 9 Gly and 18 methyl-containing residues (8 Ala, 1 Met, 5 Leu, 2 Ile and 2 Thr) were unambiguously assigned by this method. The Arg residues were identified by cross peaks arising from the NεH and the side-chain protons in the TOCSY spectra (Fig. 1, boxed cross peaks). The aromatic protons of His, Tyr and Phe were assigned from the TOCSY spectra and their Cα and Cβ protons assigned from their NOEs to the aromatic protons. The Cβ protons of the three Asn residues were identified by NOESY cross peaks to the side-chain NH protons. The three Ser residues were differentiated from Asp and Cys residues from the characteristic downfield shifts of their Cβ protons. Problems arose in differentiating Cys from Asp residues and Glu from Gln residues, which were eventually resolved by sequential assignments by NOESY.

Sequential assignments

The unique spin systems, His72, Tyr58, Phe40 and Met41, provided starting points for the sequence-specific assignments of the remaining resonances. This was achieved by comparing the COSY or TOCSY spectra in H_2O with the NOESY spectra and identifying NOESY crosspeaks between α or β proton resonances and amide proton resonances (Fig. 2). These were confirmed as sequential NOEs by checking that the spin systems matched those expected from the protein sequence. These sequence-specific assignments were further corroborated by NN (i,i+1) NOEs arising from 60–70% of the residues in the peptide. For the Xaa-Pro bonds, only $\alpha\delta$(i,i+1) connectivities were observed, without any $\alpha\alpha$ connectivities showing that the peptide bonds are all *trans*. No NOEs were observed between Cys side chains and so neither the pattern nor the conformation of the disulphide

Table 1. ^{1}H-NMR chemical shifts of albolabrin, pH 4.5, 310 K. Chemical shifts are accurate to 0.02 ppm. When only one shift is given for geminal protons, the shift for the other was not determined.

Residue	Chemical shift of				
	NH	Hα	Hβ	Hγ	others
	ppm				
Ala2	8.76	4.35	1.42		
Gly3	8.39	4.01, 3.95			
Glu4	8.11	4.38	1.62, 1.95	2.08, 2.32	
Asp5	8.48	4.63	2.66, 2.79		
Cys6	8.05	4.83	2.60, 3.34		
Asp7	8.68	4.74	2.62, 2.69		
Cys8	6.98	4.78	2.91, 3.15		
Gly9	9.29	3.98, 3.75			
Ser10	7.55	5.11	3.73, 3.98		
Pro11		4.56	2.01, 2.42	2.01	3.90, 3.92 (Hδ)
Ala12	7.83	4.29	1.34		
Asn13	7.36	4.74	2.76, 3.07		
Pro14	–	4.63 [a]			4.06, 3.87 (Hδ)
Cys15	8.71	4.64	2.51, 3.16		
Cys16	7.35	5.01	2.82, 2.92		
Asp17	8.14	4.47	2.46, 3.18		
Ala18	8.92	4.08	1.52		
Ala19	8.55	4.33	1.50		
Thr20	7.64	4.43	4.33	1.13	
Cys21	8.54 [a]	4.68 [a]	3.70		
Lys22	7.70	4.96	1.66		2.99 (Hε), 1.49, 1.93
Leu23	9.00	4.31	1.44, 1.50	1.62	0.59, 0.46 (Meδ)
Leu24	8.18	4.36	1.44	1.29	0.90, 0.84 (Meδ)
Pro25	–	4.32	2.31	–	3.85 (Hδ)
Gly26	8.53	4.14, 3.67			
Ala27	7.84	4.49	1.56		
Gln28	8.48	4.02	1.27, 0.44 [b]	2.0, 2.3 [b]	7.57, 6.85 (δNH)
Cys29	7.73	4.47	3.09, 3.21		
Gly30	9.06	4.42, 3.50			
Glu31	7.76	4.73	1.86, 2.16	2.30	
Gly32	8.32	4.81, 3.82			
Leu33	8.68	4.24	1.66	1.88	1.03, 1.02 (Meδ)
Cys34	8.44	5.39	2.73, 3.79		
Cys35	7.62	5.19	2.50, 2.99		
Asp36	9.46	4.89	2.65, 2.77		
Gln37	9.22	3.93	2.03, 2.17 [b]	2.23, 2.41 [b]	
Cys38	8.49	4.88	3.34, 3.71		
Ser39	7.95	4.92	3.70, 3.83		
Phe40	8.40	5.02	2.70, 3.00		7.21 (2,6H) 6.99 (4H), 6.98 (3,5H)
Met41	8.77	4.27	2.03, 2.32	2.67	2.14 (Hε)
Lys42	8.32	4.10	1.64 [b]	1.33 [b]	3.01 (Hε), 1.7 (Hδ)
Lys43	8.85	3.80			2.94 (Hδ), 1.6, 1.89, 1.74
Gly44	8.62	4.36, 3.41			
Thr45	7.66	4.15	3.74	1.38	
Ile46	8.95	3.99	1.72	1.73, 0.98	0.77 (Meγ), 0.89 (Meδ)
Cys47	9.13	5.05	3.02		
Arg48	7.45	4.32	1.46, 1.66 [b]	1.85, 1.86 [b]	3.27 (Hδ) 7.24 (NH)
Arg49	8.53	4.47	1.66 [b]	1.66, 1.81 [b]	3.20 (Hδ) 7.27 (NH)
Ala50	8.78	4.17	1.24		
Arg51	8.43	4.41	1.76 [b]	1.64, 1.86 [b]	3.21 (Hδ) 7.20 (NH)
Gly52	8.48	4.02, 3.80			
Asp53	8.26	4.71	2.81, 2.81		
Asp54	8.07	4.64	2.80, 280		
Leu55	8.05	4.45	1.41, 1.51	1.56	0.81, 0.76 (Meδ)
Asp56	8.02	4.60	2.30, 2.46		
Asp57	8.25	5.05	2.39, 2.95		
Tyr58	8.58	5.30	2.58, 2.66		6.92 (2,6H) 6.75 (3,5H)
Cys59	9.37	4.79	3.92, 2.54		
Asn60	9.74	4.88	2.84, 3.32		6.61, 7.62 (γNH)
Gly61	8.46	4.30			
Ile62	7.67	4.20	2.00	0.79, 0.59	0.78 (Meγ), 0.94 (Meδ)
Ser63	6.92	4.01	3.69, 3.80		
Ala64	8.86	4.28	1.80		
Gly65	7.72	4.38, 3.60			
Cys66	8.51	5.45	2.94, 2.62		
Pro67	–	4.34	1.90, 2.20	2.03	3.91, 3.78 (Hδ)
Arg68	8.23	4.14	1.56 [b]	1.66 [b]	3.15 (Hδ) 3.15 (Hε)
Asn69	8.91	4.78	2.76, 3.26		7.15, 8.20 (NH)
Pro70	–	4.47	2.35	2.02	3.94, 3.83 (Hδ)
Leu71	8.27	4.27	1.68	1.58	0.92, 0.85 (Meδ)
His72	7.96	4.62	3.26, 3.28		8.20 (2H), 7.50 (4H)
Ala73	8.14	4.13	1.36		

[a] At 300 K; [b] Tentative assignment, for the longer side chains it was not possible to distinguish between some of the side-chain protons.

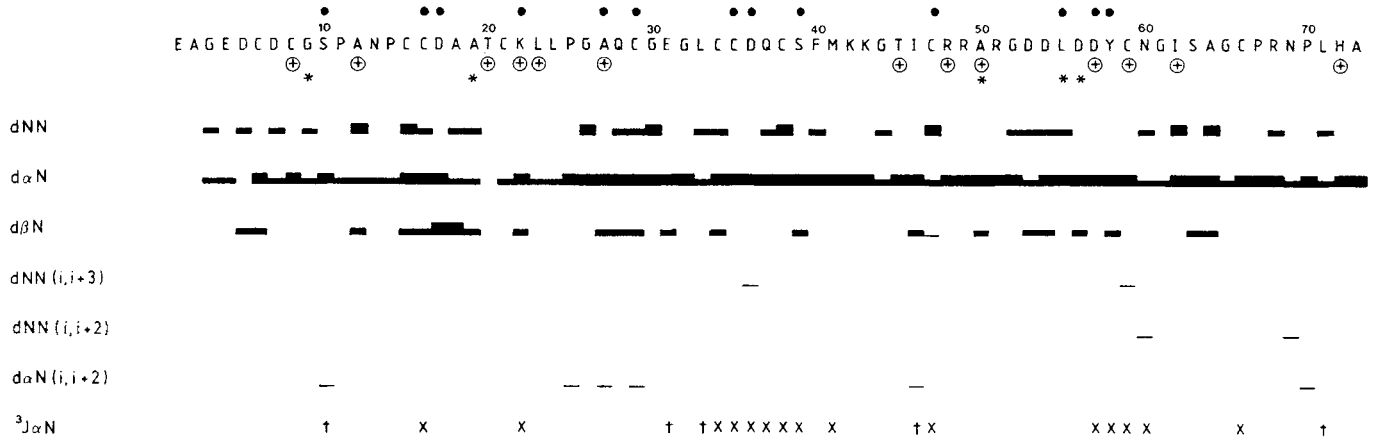

Fig. 3. Summary of the sequential and medium-range NOE connectivies, together with the coupling constants and exchange rates of the amide protons. The thickness of the lines indicate the strength of the observed NOEs. (●) Slowly exchanging NH protons, present in the two-dimensional spectrum after several hours in D_2O; (⊕) the temperature coefficient of the shift of NH protons is below 3 ppb/K; (*) the NH proton shifts by 0.04 ppm or more over the pH range 5−7; (†) $^3J_{HNH\alpha}$ below 6.5 Hz; (×) $^3J_{HNH\alpha}$ over 8 Hz.

bonds could be determined from the NMR spectra. Table 1 shows the assignment of the spectra.

Secondary structure

Few long-range NOEs were observed and only a few of the backbone coupling constants differed from those of random-coil sequence, suggesting that albolabrin contains only short sections of regular secondary structure. Fig. 3 shows the observed medium-range NOEs and backbone coupling constants, together with the slowly exchanging amide protons. The patterns of NOEs, coupling constants and exchange rates suggest that there are three turns and two segments of β sheet in the molecule, but none show all the features expected of classical secondary structure. This may be due to the disulphide bonding distorting these elements.

Residues 10−13 form the first observed turn. The strong NN connectivity between Ala12 and Asn13, $\delta\alpha$ connectivity between Pro11 and Ala12, and the low-temperature coefficient of the shift of the amide proton of Ala12 are consistent with a type II β turn, with Pro11 at the second position of the turn; however, the $^3J_{HNH\alpha}$ coupling constant of Ala12 is similar to random coil. Residues 25−31 show a series of $\alpha N(i,i+2)$ connectivities. Residues 26, 28 and 30 also give $NN(i,i+1)$ NOEs, and several of the residues have slowly exchanging amide protons and low temperature coefficients of the shifts. No $i,i+3$ NOEs are observed, so this pattern is not due to a helical structure.

The presence of long-range αN NOEs, large $^3J_{HNH\alpha}$ values, downfield shifted CαH resonances, and slowly exchanging NH protons suggests that there are two short sections of two-stranded antiparallel β sheet. One, extemely short, links residues 34, 35 and 36 with residues 40 and 41. The cross-strand NH-CαH NOEs observed are shown in Fig. 2. An additional NOE is observed between Asp36 NH and Ser39 NH; residues 37−39 therefore form a tight reverse turn. This turn does not show the NOEs expected from either a type I or a type II turn and has $^3J_{HNH\alpha}$ values of 9.2 Hz and 8.5 Hz, respectively, for residues 37 and 38. The other β sheet links residues 43−50 with 56−61 (Figs 2 and 4C, D). All the cross-strand NH-CαH NOEs observed for this sheet are shown in Fig. 2. In addition, there is an NOE between Ile46 CαH and Tyr58 CαH. There is a bulge at residues 46−48 indicated by an $\alpha N(i,i+2)$ connectivity between Ile46 and Arg48, also shown in Fig. 2, and the coupling constants of residues 46, 48 and 49 are small for an extended conformation (Fig. 3), thus this sheet is distorted. At residue 61 there is a turn bringing the C-terminal tail close to the β sheet. One NOE, between the amide protons of residues Asn60 and Ile62, is observed together with a longer-range NOE between Asn69 NH and either Asp57 or Cys47 CαH, which overlap. Residues 69−72 form a final turn, with Pro70 as residue 2. This is close to a type II β turn.

The RGD recognition site lies at residues 51−53, in the loop between the strands of the second β sheet lying at residues 50−56. At the end of the β sheet there is an NOE between Ala50 NH and Asp56 CαH (Fig. 4C) and in the loop the only medium-range NOEs are between Ala50 βCH_3 and both Asp54 CαH and Asp56 CαH (Fig. 4A, B), a weaker NOE is observed between Ala50 βCH_3 and Leu55 CαH which may be due to spin diffusion from the Leu55 NH. Weak $NN(i,i+1)$ connectivities are observed in this loop and the $^3J_{HNH\alpha}$ values range between 6.8−8.0 Hz, suggesting that the loop is mobile and that the turn is transient in nature.

pH dependence

On raising the pH from 5.0 to 7.0 most of the amide proton resonances decrease in intensity, as would be expected from increased exchange with the solvent. A few of the amide protons shift downfield, the largest changes in shift being observed for Gly9 NH (0.08 ppm), Ala19 NH (0.15 ppm) and Ala50 NH (0.20 ppm) downfield (Figs 3 and 4C, D). The large downfield change in shift of Ala50 NH is combined with a 0.05-ppm downfield shift for Leu55 NH and a 0.05-ppm upfield shift of Ala50 CαH. No additional NOEs were observed in the spectrum at pH 7.0, but the NOE between Ala50 NH and Asp56 CαH, at the top of the loop, was no longer observed (cf. Fig. 4C, D). There was no weakening of other NOEs from either resonance, e.g. the NOE between Ala50 NH and Ala50 βCH_3 (Fig. 4C, D), or between Ala50 βCH_3 and Asp56 CαH (Fig. 4A, B), showing that the loss of the NOE is not due to broadening of the peaks. This suggests that the neck of the RGD loop may move apart at neutral pH. This, together with the other downfield shifts observed,

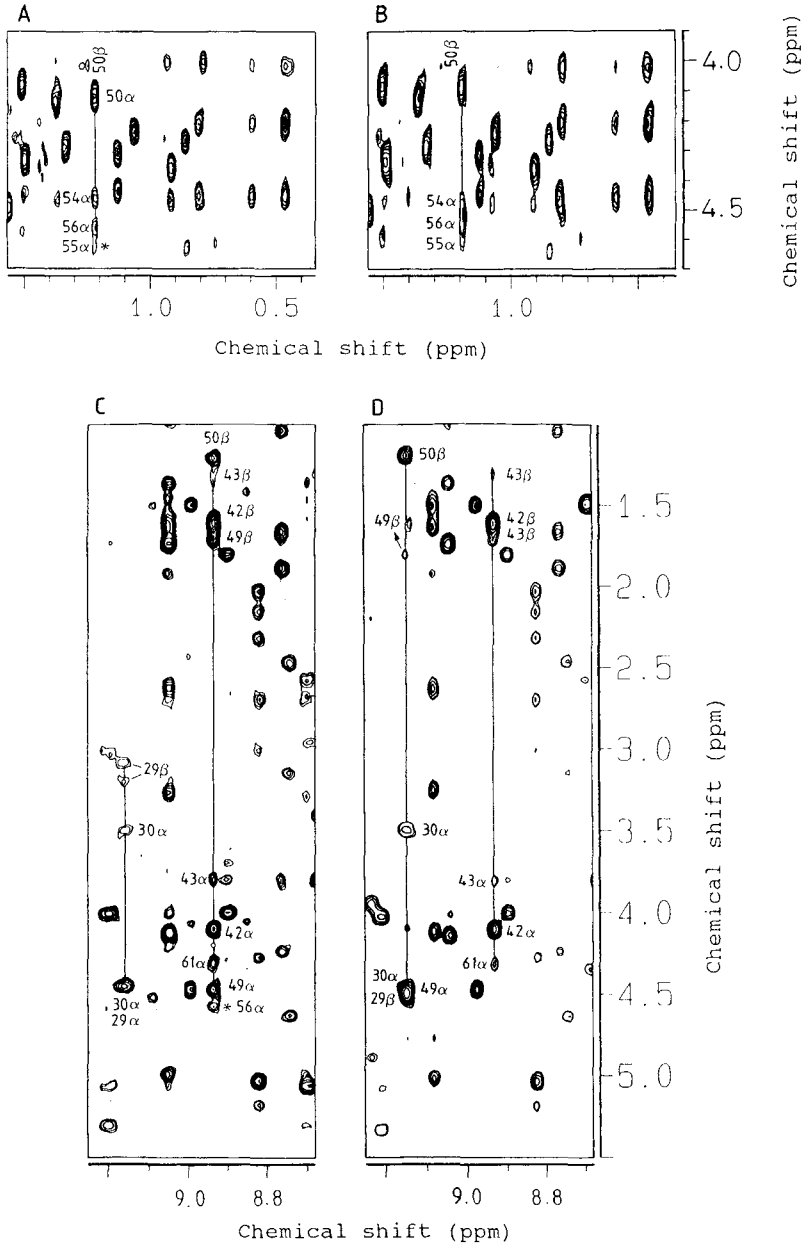

Fig. 4. pH dependence of the NOE between Ala50 NH and Asp56 CαH. (A) Section of the NOESY spectrum of albolabrin in H_2O, pH 5.0, 300 K, recorded with mixing time 150 ms, showing the NOE between Ala50 βCH_3 at 1.22 ppm and Asp54 CαH, Leu55 CαH and Asp56 CαH resonances. (B) Equivalent region of the NOESY spectrum of albolabrin at pH 7.0, recorded with mixing time 150 ms, showing the same connectivities. (C) Section of the NOESY spectrum of albolabrin in H_2O, pH 5.0, 300 K, recorded with mixing time 150 ms, showing the NOEs from Ala50 NH to Ala50 βCH_3, Asp56 CαH, Arg49 CαH and Arg49 CβH resonances at 8.95 ppm. Lys43 NH also resonates at this position and its NOEs to Lys42 CαH, Lys43 CβH and across the strand to Gly61 CαH are also marked. Gly30 NH resonates at 9.16 ppm and its NOEs to Gly30 CαH and Cys29 CβH are marked. (D) Section of the NOESY spectrum of albolabrin in H_2O, pH 7.0, 300 K, recorded with mixing time 150 ms, showing the NOEs from Ala50 NH to Ala50 βCH_3, Ala50 CαH and Arg49 CαH at 9.14 ppm. This now overlaps with the Gly30 NH resonance and its NOEs and those of Lys43 NH are also marked.

may be influenced by ionisation of neighbouring Asp residues over this pH range. The only change in shift observed for these over this pH range is a small 0.04-ppm upfield shift of one of the β protons of Asp56.

Comparison with kistrin and echistatin

Albolabrin is highly similar to both kistrin and echistatin (Fig. 5). The N-terminal amino acids 6–40 show only five amino acids changes from kistrin, while residues 44–70 differ in only six amino acids from echistatin. The secondary structure of echistatin has been determined independently by four groups (Saudek et al., 1991b; Cooke et al., 1991; Dalvit et al., 1991; Chen et al., 1991) and two have subsequently reported its tertiary structure (Saudek et al.,1991a; Cooke et al.,1992). The secondary and tertiary structures of kistrin have been reported by Wagner and coworkers in two papers (Adler et al., 1991; Adler and Wagner, 1992). The main features described by the four groups for echistatin are in broad agreement with some slight differences in nomenclature,

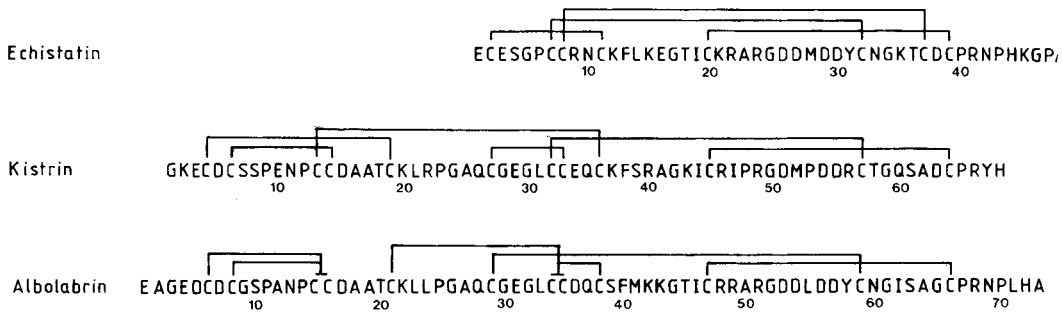

Fig. 5. Amino-acid sequence and disulphide-bonding comparison between the disintegrins echistatin, kistrin and albolabrin. The sequences of these peptides were determined by Dennis et al. (1990), Gan et al. (1988) and Williams et al. (1990b). The disulphide-bonding pattern is taken from Calvete et al. (1992), Adler and Wagner (1993) and Calvete et al. (1991).

possibly because the features do not correspond exactly to regular secondary structure. These structural elements also agree with the features observed in the C-terminal portion of kistrin, although in the latter it is stressed that the NOEs observed are not consistent with classical secondary structure. The elements of secondary structure observed in albolabrin for the residues 38–73 are similar to those reported for echistatin and for kistrin.

Like these two other disintegrins, albolabrin appears to have a very mobile structure primarily constrained by the disulphide-bonding. The NMR data obtained gives no independent evidence for the disulphide bonding pattern in albolabrin. All the observed NOEs are consistent with the disulphide bonding determined by Calvete et al. (1991). However, in this family of proteins, the energy differences and root-mean-square deviations of structures calculated from NOEs for alternative disulphide-bonding patterns are small (Adler et al., 1993; Cooke et al., 1992; Klaus et al., 1993), so other disulphide patterns cannot be excluded from the NMR data. The N-terminal 20 amino acids of albolabrin give no NOEs to the remainder of the molecule, suggesting that they move independently of the core of the protein. This is consistent with the existence of the shorter disintegrins with similar potency, such as echistatin. It contrasts with the NOEs observed in kistrin between Cys13 and Cys36, defining a cystine bridge between them.

The first bend observed in albolabrin at residues Ser10–Asn13, corresponds to that between Ser8–Asn11 in kistrin, but in the latter a second bend between Asn11–Cys14 is also observed. The short section of β sheet at residues 34–43 in albolabrin correspond to residues 8–14 in echistatin where there is a turn and some authors report a short β sheet here. In kistrin, these turns and possible β sheet occur a few residues earlier, at Gly30–Cys33 and Glu34–Lys37.

All groups suggest that the RGD sequence is in the loop of a segment of irregular β sheet. In kistrin, the β sheet was proposed to run between 41–47 and 52–59 but contradictory NOEs were seen and the last long-range backbone–backbone NOE shown is between residues 46 and 55, equivalent to residues 48 and 57 in albolabrin (Adler et al., 1991; Adler and Wagner, 1992). In echistatin, the β sheet and β bulge links residues 16–20 with 30–33 so the loop is between 21–30; again equivalent to 48–57 in albolabrin (Dalvit et al., 1991; Chen et al., 1991; Cooke et al., 1991, 1992; Saudek et al., 1991a, b). The NOE at the end of the stem of the β sheet between Cys20 NH and Tyr31 CαH, observed in all the studies of echistatin, is equivalent to that between Cys47 NH and Tyr58 CαH in albolabrin (Fig. 2). However, in albolabrin, at low pH, we also observe a backbone–backbone NOE between Ala50 NH and Asp56 CαH (Fig. 4C). This NOE is not observed in the other disintegrins and extends the β sheet further towards the RGD sequence than in the other disintegrins.

Within the loop in echistatin, Chen et al. (1991) and Cooke et al. (1991) have reported changes in the shifts of Ala23 resonances with pH in echistatin, together with other smaller effects on shifts, equivalent to the change in shift of Ala50 seen in albolabrin. Different groups report NOEs between Ala23 βCH_3 and Asp27, Met28 and Asp29 (Dalvit et al., 1991; Cooke et al., 1991; Saudek et al., 1991b), the exact NOEs varying slightly. These are similar to the NOEs observed between Ala50 βCH_3 and Asp54 CαH, Leu55 CαH, and Asp56 CαH in albolabrin (Fig. 4A, B). Thus it seems that the loop conformation in echistatin and albolabrin may be similar at high pH.

There appears to be a turn after the β sheet in echistatin, whereas in kistrin the conformation of the residues after the sheet is described as a broad loop and the C-terminal residues are ill defined.

CONCLUSION

The ^{1}H-NMR spectrum of albolabrin has been assigned and an outline of its secondary structure discussed. The C-terminal part of the molecule appears to have a similar local structure to echistatin and kistrin. Calculations of the tertiary structure of albolabrin are now under way to define better the secondary structure elements observed and, as far as possible, the overall structure. The additional NOE observed in the RGD region may allow better definition of this loop in albolabrin than in the other disintegrins.

The work described was supported by grants from The Wellcome Trust and the Science and Engineering Research Council (UK). The NMR centre at the University of Birmingham was set up with funds from The Wellcome Trust, the Science and Engineering Research Council and the Arthritis and Rheumatism Council. We thank Dr. Y. Gao and Mr. A. J. Pemberton for skilful maintenance of the instrumentation.

REFERENCES

Adler, M. & Wagner, G. (1992) Sequential ^{1}H-NMR assignments of kistrin, a potent platelet aggregation inhibitor and glycoprotein IIb-IIIa antagonist, *Biochemistry 31*, 1031–1039.

Adler, M., Lazarus, R. A., Dennis, M. S. & Wagner, G. (1991) Solution structure of kistrin, a potent platelet aggregation inhibitor and glycoprotein IIb-IIIa antagonist, *Science 253*, 445–448.

Adler, M., Carter, P., Lazarus, R. A. & Wagner, G. (1993) Cysteine pairing in the glycoprotein IIbIIa antagonist kistrin using NMR, chemical analysis and structure calculations, *Biochemistry 32*, 282–289.

Babul, J. & Stellwagen, E., (1969) Measurement of protein concentration with interferences optics, *Anal. Biochem. 28*, 216–221

Bax, A. & Davis, D. G. (1985) MLEV-17 based 2D homonuclear magnetisation transfer spectroscopy, *J. Magn. Reson. 65*, 355–360.

Braunschweiler, L. & Ernst, R. R. (1983) Coherence transfer by isotopic mixing – application to proton correlation spectroscopy, *J. Magn. Reson. 53*, 521.

Calvete, J. J., Schafer, W., Soszka, T., Lu, W., Cook, J. J., Jameson, B. A. & Niewiarowski, S. (1991) Identification of the disulfide bond pattern in albolabrin, an RGD-containing peptide from the venom of *Trimeresurus albolabris*: significance for the expression of platelet aggregation inhibitory activity, *Biochemistry 30*, 5225–5229.

Calvete, J. J., Wang, Y., Mann, K., Schafer, W., Niewiarowski, S. & Stewart, G. J. (1992) The disulfide bridge pattern of snake venom disintegrins, flavoridin and echistatin, *FEBS Lett. 3*, 316–320.

Chen, Y., Pitzenberg, S. M., Garsky, V. M., Lumma, P. K., Sanyal, G. & Baum, J. (1991) Proton NMR assignments and secondary structure of the snake venom protein echistatin, *Biochemistry 30*, 11,625–11,636.

Chervenka, C. H. (1970) Long-column meniscus depletion sedimentation equilibrium technique for the analytical ultracentrifuge, *Anal. Biochem 34*, 24–49.

Cohn, E. J. & Edsall, J. T. (1943) *Proteins, amino acids & peptides*, pp. 370–381, Reinhold Publishing Corporation, New York.

Cooke, R. M., Carter, B. G., Martin, D. M. A., Murray-Rust, P. & Weir, M. P. (1991) Nuclear magnetic resonance studies of the snake toxin echistatin – ^{1}H resonance assignments and secondary structure, *Eur. J. Biochem. 202*, 323–328.

Cooke, R. M., Carter, B. G., Murray-Rust, P., Hartshorn, M. J., Herzyk, P. & Hubbard, R. E. (1992) The solution structure of echistatin: evidence for disulphide bond rearrangement in similar snake toxins, *Protein Eng. 5*, 473–477.

Dalvit, C., Widmer, H., Bovermann, G., Breckenridge, R. & Metternich, R. (1991) ^{1}H NMR studies of echistatin in solution – sequential resonance assignments and secondary structure, *Eur. J. Biochem. 202*, 315–321.

Dennis, M. S., Henzel, W. J., Pitti, R. M., Lipari, M. T., Napier, M. A., Deisher, T. A., Bunting, S. & Lazarus, R. A. (1990) Platelet glycoprotein IIb-IIIa antagonists from snake venoms: evidence for a family of platelet aggregation inhibitors, *Proc. Natl Acad. Sci. USA 87*, 2471–2475.

Gan, Z. R., Gould R., J., Jacobs, J. W., Friedman, P. A. & Polokoff, M. A. (1988) Echistatin, *J. Biol. Chem 263*, 19827–19832.

Gartner, T. K. & Bennett, J. S. (1985) The tetrapeptide analog of the cell attachment site of fibronectin inhibits platelet aggregation and fibrinogen binding to activated platelets, *J. Biol. Chem. 260*, 11891–11894.

Gould, R. J., Polokoff, M. A., Friedman, P. A., Huang, T.-F., Cook, J. J. & Niewiarowski, S. (1990) Disintegrins, a family of integrin inhibitory proteins from viper venoms, *Proc. Soc. Exp. Biol. Med. 195*, 168–171.

Huang, T.-F. Holt, J. C., Lukasiewicz, H. & Niewiarowski, S. (1987) Trigamin, *J. Biol. Chem. 262*, 16157–16163.

Huang, T.-F., Holt, J. C., Kirby, E. P. & Niewiarowski, S. (1989) Trigramin: primary structure and its inhibition of von Willebrand factor binding glycoprotein IIb/IIIa complex of human platelets, *Biochemistry 28*, 661–668.

Jeener, J., Meier, B. H., Bachmann, P. & Ernst, R. R. (1979) Investigation of exchange processes by two-dimensional exchange spectroscopy, *J. Chem. Phys. 71*, 4546–4553.

Klaus, W., Broger, C., Gerber, P. & Senn, H. (1993) Determination of the disulphide bonding pattern in proteins by local and global analysis of nuclear magnetic resonance data; application to flavoridin, *J. Mol. Biol. 232*, 897–906.

Kumar, R. M., Ernst, R. R. & Wuthrich, K. (1980) A two dimensional nuclear Overhauser enhancement (2D NOE) experiment for the elucidation of complete proton–proton cross relaxation networks in biological macromolecules, *Biochem. Biophys. Res. Commun. 95*, 1–6.

Marion, D. & Wuthrich, K. (1983) Application of phase sensitive two dimensional correlated spectroscopy (COSY) for measurements of ^{1}H-^{1}H spin-spin coupling constants in proteins, *Biochem. Biophys. Res. Commun. 113*, 967–974.

Piantini, U., Sorenson, O. W. & Ernst, R. R. (1982) Multiple quantum filters for elucidating NMR coupling networks, *J. Am. Chem. Soc. 104*, 6800–6801.

Plow, E. F., Pierschbacher, M. D., Ruoslahti, E., Marguerie, G. & Ginsberg, M. H. (1985) The effect of arg-gly-asp containing peptides on fibrinogen and von Willebrand factor binding to platelets, *Proc. Natl Acad. Sci. USA 82*, 8057–8061.

Plow, E. F., Pierschbacher, M. D., Ruoslahti, E., Marguerie, G. & Ginsberg, M. H. (1987) Arginyl-glycyl-aspartic acid sequences and fibrinogen binding to platelets, *Blood 70*, 110–115.

Rance, M., Sorenson, O. W., Bodenhausen, G., Wagner, G., Ernst, R. R. & Wuthrich, K. (1983) Improved spectral resolution in COSY ^{1}H-NMR spectra of proteins via double quantum filtering, *Biochem. Biophys. Res. Commun. 117*, 479–485.

Ruoslahti, E. & Pierschbacher, M. D. (1987) New perspectives in cell adhesion – RGD and integrins, *Science 227*, 491–479.

Samanen, J., Ali F., Romoff, T., Calvo, R., Sorenson, E., Vasko, J., Storer, B., Berry, D., Bennett, D., Strohsacker, M., Powers, D., Stadel, J. & Nichols, A. (1991) Development of a small RGD peptide fibrinogen receptor antagonist with potent antiaggregatory activity in vitro, *J. Med. Chem. 34*, 3114–3125.

Saudek, V., Atkinson, R. A. & Pelton, J. T. (1991a) Three-dimensional structure of echistatin, the smallest active RGD protein, *Biochemistry 30*, 7369–7372.

Saudek, V., Atkinson, R. A., Lepage, P. & Pelton, J. T. (1991b) The secondary structure of echistatin from ^{1}H-NMR, circular dichroism and Raman spectroscopy, *Eur. J. Biochem. 202*, 329–338.

Scarborough, R. M., Rose, J. W., Naughton, M. A., Philips, D. R., Nannizzi, L., Arfsten, A., Cambell, A. M. & Charo, I. F. (1993) Characterization of the integrin specificities of disintegrins isolated from American pit viper venoms, *J. Biol. Chem. 268*, 1058–1065.

Senn, H. & Klaus, W. (1993) The nuclear magnetic resonance structure of flavoridin, an antagonist of the platelet Gp IIb-IIIa receptor, *J. Mol. Biol. 234*, 907–925.

Shaka, A. J. & Freeman, R. (1983) Simplification of NMR spectra by filtration through multiple-quantum coherence, *J. Magn. Reson. 51*, 169–173.

Williams, J. A. (1992) Disintegrins: RGD-containing proteins which inhibit cell/matrix (adhesion) and cell/cell (aggregation) interactions via the integrin receptors, *Pathol. Biol. 40*, 813–821.

Williams, J. A., Ashby, B. & Daniel, J. L. (1990a) Ligands to the platelet fibrinogen receptor glycoprotein IIb-IIIa do not affect agonist-induced second messengers Ca^{2+} or cyclic AMP, *Biochem. J. 270*, 149–155.

Williams, J. A., Rucinski, B., Holt, J. & Niewiarowski, S. (1990b) Elegantin and albolabrin purified peptides from viper venoms: homologies with the RGDS domain of fibrinogen and von Willebrand factor, *Biochim. Biophys. Acta 1039*, 81–89.

Wuthrich, K. (1986) *NMR of proteins and nucleic acids*, Wiley-Interscience, New York.